Int. J. Heat Mass Transfer. Vol. 32, No. 12, pp. 2447–2457, 1989
Printed in Great Britain

0017–9310/89 $3.00 + 0.00
© 1989 Pergamon Press plc

The problem of time-dependent natural convection melting with conduction in the solid

ZONGQIN ZHANG and ADRIAN BEJAN
Department of Mechanical Engineering and Materials Science, Duke University, Durham, NC 27706, U.S.A.

(*Received* 28 *October* 1988 *and in final form* 14 *March* 1989)

Abstract—This paper reports a theoretical and experimental study of the effect of solid-side subcooling on the phenomenon of melting by natural convection at the vertical interface between a solid body and a pool of its own liquid. The first part of the study consists of a conjugate boundary layer analysis of the transient melting process, in which the effect of solid subcooling leads to the formation of a time-dependent conduction boundary layer in the solid. The theoretical solution documents not only the effect of solid subcooling on the melting rate, but also the effects of liquid superheating (Stefan number) and thermal diffusivity ratio. The second part of the study consists of melting experiments conducted in a rectangular enclosure heated at a constant rate from the side. The solid subcooling parameter B covers the range 0.3–6.3, as the Rayleigh number remains fixed. The experiments show that in the conduction-dominated regime the Nusselt number increases as B increases. In the convection-dominated regime, the effect of the subcooling parameter B is insignificant. It is shown that these experimental observations agree with the trends anticipated theoretically in the first part of the study.

1. INTRODUCTION

THE OBJECTIVE of the present study is to document the effect of solid subcooling on melting in the presence of natural convection. The configuration consists of a block of subcooled solid that is instantaneously placed in thermal communication with a semi-infinite pool of quiescent superheated liquid. The solid and the liquid are phases of the same pure substance. The thermal communication between the two phases leads to the development of time-dependent thermal boundary layers on both sides of the solid–liquid interface. The wall jet flow induced along the liquid side of the interface is also time dependent.

From a fundamental standpoint, the time-dependent boundary-layer melting problem described above is a generalization of a related class of problems that have been examined in the steady state. Recent examples of steady-state boundary-layer melting problems are the laminar forced convection and laminar film condensation melting considered by Epstein and Cho [1, 2], and the forced-convection melting of permafrost considered by Reid [3].

Our own interest in the time-dependent melting problem was triggered by the continuing effort [4, 5] to correlate the melting rate data from experiments involving enclosed phase-change materials. The pre-1984 literature in this area was reviewed by Viskanta [6]; some of the representative experimental and numerical studies are listed chronologically in refs. [7–14].

A plausible explanation for some of the disagreement between the various sets of melting rate data, especially between those obtained in the early period of the melting process, is the effect of time-dependent conduction into the solid phase. This effect is present when the initial temperature of the solid is lower than the melting point, i.e. when the degree of subcooling is finite. Kassinos and Prusa [15] have shown that the effect of finite subcooling is to decrease the instantaneous melting rate below the value that is registered in the case when the solid remains isothermal and at the melting point. Kassinos and Prusa demonstrated this effect in the context of an enclosed phase-change material that is suddenly heated along a solid and impermeable side wall. In order to focus exclusively on the interaction between solid-body conduction and natural convection at the two-phase interface, in the present problem we assume that the liquid pool is semi-infinite and isothermal.

2. PHYSICAL MODEL

According to Fig. 1, the focus of the analysis is on the temperature and flow fields that develop near the vertical interface between a solid and its own liquid, when the two are placed suddenly in thermal communication. Initially, the solid block is isothermal (T_s), while the pool of liquid is both isothermal (T_f) and quiescent. The solid and liquid temperatures embrace the melting point (T_m) of the two-phase interface, $T_s < T_m < T_f$. In other words, the configuration is characterized by both liquid superheating ($\Delta T_f = T_f - T_m$) and solid subcooling ($\Delta T_s = T_m - T_s$).

An essential feature of the model is the x–y system of coordinates, which is *attached* to the two-phase interface. In this system, the rate at which the interface

NOMENCLATURE

A	thermal diffusivity ratio, equation $(13)_2$
B	solid subcooling parameter, equation (17)
c_f	specific heat of solid
C	instantaneous, height-averaged cooling rate (conduction into the solid), equation (24)
F	function, $\tilde{\delta}^2$
g	gravitational acceleration
G	function, $\tilde{\lambda}^2$
h_{sf}	latent heat of fusion
H	height
He	instantaneous, height-averaged heating rate (convection from the liquid), equation (23)
k_f	thermal conductivity of liquid
k_s	thermal conductivity of solid
M	instantaneous, height-averaged melting rate, equation (22)
N	number of steps in the vertical direction, Table 1
Nu	Nusselt number, equation (28)
Pr	Prandtl number
q''	heat flux
Ra	Rayleigh number based on temperature difference, equation (9)
Ra_*	Rayleigh number based on heat flux, equation (27)
s	deflection of the two-phase interface, Section 9
S	volume swept by the two-phase interface, equation (26)
Ste	Stefan number (liquid superheat), equation (16)
t	time
$\Delta\tilde{t}$	time step, Table 1
T	temperature
T_{avg}	average temperature of the heated wall
T_f	temperature of the liquid pool
T_m	melting point
T_s	temperature of the solid
ΔT_f	degree of liquid superheating, $T_f - T_m$
ΔT_s	degree of solid subcooling, $T_m - T_s$
u	horizontal velocity component
u_0	melting velocity, equation (14)
v	vertical velocity component
V	function, equation (5)
x	horizontal coordinate
y	vertical coordinate.

Greek symbols

α_f	liquid thermal diffusivity
α_s	solid thermal diffusivity
β	volumetric coefficient of thermal expansion
δ	thickness of liquid natural convection boundary layer
θ_*	dimensionless time, equation (29)
λ	thickness of solid conduction boundary layer
ν	kinematic viscosity
ρ	density of liquid or solid.

Superscript

$\tilde{(\ )}$	dimensionless variables defined in equations (7) and (8).

advances by melting into the solid appears as a 'blowing' velocity u_0, that is, as the velocity of the liquid that is generated at the interface and pushed to the right, into the liquid boundary layer that descends along the interface.

Related to this feature is the assumption that the life of the melting process is sufficiently short, so that the interface remains nearly straight over most of its height H. In its earliest stages the interface is indeed straight, as the heat transfer process is ruled by pure conduction on both sides of the interface. As the time increases, the liquid-side boundary layer eventually becomes 'convective', in other words, it develops into a vertical flow the mission of which is to bring to each y location on the interface the heating effect that fuels the melting process. It is well known that the effect of convection is to distribute the heat transfer unevenly, so that the uppermost portion of the interface melts faster than the rest. In time, the interface and the y-axis of Fig. 1 develop a curvature that is most pronounced near the top (starting point) of the liquid boundary layer. This deformation, of course, threatens the validity of the analysis: in Section 9 we develop a criterion for the time domain in which the boundary-layer description is sufficiently accurate.

The physical modeling is completed by assuming that the liquid is Newtonian and Boussinesq incompressible. Its properties are treated as constant in all cases except in the buoyancy term of the momentum equation, in which the usual linear relation is assumed between small changes in density and small isobaric changes in temperature. The solid is homogenous and isotropic. Its thermal conductivity (k_s) and thermal diffusivity (α_s) are not necessarily the same as the corresponding properties of the liquid phase (k_f, α_f). However, the density of the solid is assumed to equal the density of the liquid (ρ).

3. CONJUGATE BOUNDARY LAYERS

The analysis consists of developing time-dependent solutions for the thermal boundary layers that form

on the two sides of the interface, and then matching these two solutions across the interface. The thermal boundary-layer solution for the liquid side demands also a solution for the flow field. The liquid-side problem reduces to solving the conservation statements for mass, momentum and energy

$$\frac{\partial u}{\partial x}+\frac{\partial v}{\partial y}=0 \tag{1}$$

$$v\frac{\partial^2 v}{\partial x^2}+g\beta(T-T_f)=0 \tag{2}$$

$$\frac{\partial T}{\partial t}+\frac{\partial}{\partial x}(uT)+\frac{\partial}{\partial y}(vT)=\alpha_f\frac{\partial^2 T}{\partial x^2}. \tag{3}$$

The last two of these equations have been simplified in accordance with the boundary-layer slenderness assumption, $\delta < H$, where δ is the thermal boundary-layer thickness. It has been assumed also that the liquid has a Prandtl number the order of magnitude of which is greater than 1 : this assumption is sufficient for neglecting the inertia terms in equation (2). That equation is valid inside the thermal boundary layer, where the effect of inertia is negligible relative to that of buoyancy and friction (see, e.g. p. 117 of ref. [16]).

Equations (1)–(3) were solved by using the integral method, which has been used extensively in earlier treatments of boundary-layer phase-change problems (e.g. refs. [1–3, 17]). The assumed temperature and vertical velocity profiles were the same as Squire's [18]

$$T=T_f-\Delta T_f\left(1-\frac{x}{\delta}\right)^2 \tag{4}$$

$$v=V\frac{x}{\delta}\left(1-\frac{x}{\delta}\right)^2. \tag{5}$$

These profiles were chosen because, relative to other profile expressions, they lead to more accurate integral results in boundary-layer natural convection [19]. They compare well with the exact shapes of the profiles found in natural convection with blowing through the vertical wall [20].

The actual integral analysis is omitted for the sake of brevity. It begins with integrating equation (2) from $x=0$ to δ, in order to evaluate the velocity coefficient $V(y,t)$. Next, corresponding integrals of the mass and energy equations are found to contain as unknowns the horizontal velocities at the edges of the boundary layer, namely, the blowing (melting) velocity at the interface, u_0, and the entrainment velocity u_δ at the outer edge. Eliminating u_δ between these last two equations yields a single equation in terms of only $u_0(y,t)$ and $\delta(y,t)$

$$\frac{1}{3}\frac{\partial\tilde{\delta}}{\partial\tilde{t}}-\tilde{u}_0+\frac{1}{90}\frac{\partial(\tilde{\delta}^3)}{\partial\tilde{y}}=\frac{2}{\tilde{\delta}} \tag{6}$$

where the dimensionless variables are defined as

$$\tilde{y}=-\frac{y}{H},\quad \tilde{\delta}=\frac{\delta}{H}Ra^{1/4} \tag{7}$$

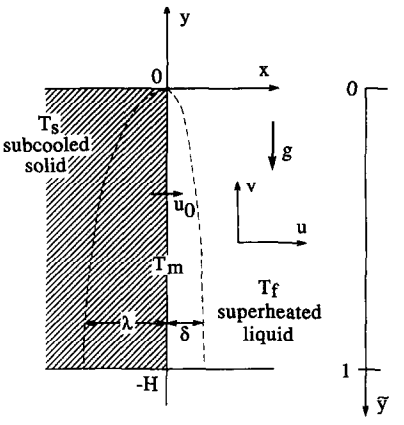

FIG. 1. Conjugate boundary layers at the interface between a subcooled solid and a superheated pool of its own liquid.

$$\tilde{u}_0=u_0\frac{H}{\alpha}Ra^{-1/4},\quad \tilde{t}=t\frac{\alpha_f}{H^2}Ra^{1/2} \tag{8}$$

$$Ra=\frac{g\beta\Delta T_f H^3}{\alpha_f\nu}. \tag{9}$$

Worth noting in this nondimensionalization is the use of the proper scales of the *transient* thermal boundary layer in a high Prandtl number fluid. In particular, the time scale $(H^2/\alpha_f)Ra^{-1/2}$ is associated with the time when the liquid boundary-layer flow reaches its steady state, i.e. a balance between buoyancy and friction in the thermal boundary layer (pp. 160–164 of ref. [16]). The minus sign in the definition of $\tilde{y}$ means that the dimensionless boundary layer stretches from $\tilde{y}=0$, at the top, to $\tilde{y}=1$ at the bottom of the two-phase interface.

The analysis of the thermal boundary layer that develops on the solid side of the interface is even simpler, because in this case the 'flow' of the solid medium is known. That flow field is represented by the horizontal velocity $u_0(y,t)$, with which the solid approaches and eventually crosses the y-axis (Fig. 1). The boundary-layer simplified energy equation for the solid phase is therefore

$$\frac{\partial T}{\partial t}+u_0\frac{\partial T}{\partial x}=\alpha_s\frac{\partial^2 T}{\partial x^2}. \tag{10}$$

The corresponding Squire-type temperature profile for the solid side is

$$T=T_s+\Delta T_s\left(1+\frac{x}{\lambda}\right)^2 \tag{11}$$

showing that the boundary layer extends from $x=0$ to $-\lambda$, where the thickness λ is a function of both y and t. Ultimately, the integral of the energy equation (10) reduces to

$$\frac{1}{3}\frac{\partial\tilde{\lambda}}{\partial\tilde{t}}+\tilde{u}_0=\frac{2A}{\tilde{\lambda}} \tag{12}$$

in which the new dimensionless variables are

$$\tilde{\lambda} = \frac{\lambda}{H} Ra^{1/4}, \quad A = \frac{\alpha_s}{\alpha_f}. \tag{13}$$

Parameter A accounts for the fact that the thermal diffusivity of the solid may differ from that of the liquid.

The two equations developed so far, equations (6) and (12), contain a total of three unknowns ($\tilde{u}_0, \tilde{\delta}, \tilde{\lambda}$). The problem is closed by recognizing the first law of thermodynamics for the control volume of zero thickness that encloses the two-phase interface (see, e.g. p. 857 of Viskanta [6])

$$\rho h_{sf} u_0 = k_f \left(\frac{\partial T}{\partial x}\right)_{0^+} - k_s \left(\frac{\partial T}{\partial x}\right)_{0^-}. \tag{14}$$

The right-hand side of this equation expresses the difference between the heat flux delivered by the liquid boundary layer, and the heat flux absorbed by the solid boundary layer. The dimensionless counterpart of this energy continuity condition is

$$\tilde{u}_0 = 2Ste\left(\frac{1}{\tilde{\delta}} - \frac{B}{\tilde{\lambda}}\right) \tag{15}$$

in which Ste is the liquid-superheat Stefan number

$$Ste = \frac{c_f \Delta T_f}{h_{sf}} \tag{16}$$

and B is a dimensionless group that accounts primarily for the effect of solid subcooling

$$B = \frac{k_s \Delta T_s}{k_f \Delta T_f}. \tag{17}$$

The subcooling parameter B was identified by Yao and Cherney [21] (parameter 'Sb' in their notation), and used subsequently by Prusa and Yao [22], as well as Kassinos and Prusa [15]. The make up of this group is important, because it shows that the conductivity ratio k_s/k_f does not appear as an independent dimensionless group.

4. SOLUTION

In summary, the problem consists of solving equations (6), (12) and (15) for three functions of $\tilde{y}$ and $\tilde{t}$, namely, $\tilde{u}_0$, $\tilde{\delta}$ and $\tilde{\lambda}$. The initial and boundary conditions are the statements that the liquid and solid phases are initially isothermal

$$\tilde{\delta} = \tilde{\lambda} = 0 \quad \text{at} \quad \tilde{t} = 0 \tag{18}$$

and that the liquid boundary-layer flow starts from the top of the interface

$$\tilde{\delta} = 0 \quad \text{at} \quad \tilde{y} = 0. \tag{19}$$

This problem was solved numerically by first eliminating $\tilde{u}_0$ between equations (6), (12) and (15), and introducing the new variables $F = \tilde{\delta}^2$ and $G = \tilde{\lambda}^2$. The two equations that emerge are

$$\frac{\partial F}{\partial \tilde{t}} - 12Ste\left[1 - B\left(\frac{F}{G}\right)^{1/2}\right] + \frac{F}{10}\frac{\partial F}{\partial \tilde{y}} = 12 \tag{20}$$

$$\frac{\partial G}{\partial \tilde{t}} + 12Ste\left[\left(\frac{F}{G}\right)^{1/2} - B\right] = 12A. \tag{21}$$

The $\tilde{y}$ interval [0, 1] was divided into $N = 41$ equal steps, and the time step was set at $\Delta\tilde{t} = 0.01$. Finite-difference versions of equations (20) and (21) were solved by the Euler implicit method, and, respectively, by the first-order explicit method. The accuracy of the numerical solution is documented in Table 1, which shows that the chosen steps (the bottom row) are sufficiently fine.

The main features of the time-dependent solution are illustrated in Fig. 2 in terms of three height-averaged quantities, the instantaneous melting rate

$$M(\tilde{t}) = \frac{1}{Ste}\int_0^1 \tilde{u}_0(\tilde{y}, \tilde{t})\, d\tilde{y} \tag{22}$$

the instantaneous 'heating' rate, or the heat transfer from the liquid-side boundary layer to the two-phase interface

$$He(\tilde{t}) = \int_0^1 \frac{2}{\tilde{\delta}} d\tilde{y} \tag{23}$$

and the instantaneous 'cooling' rate, or the conduction heat transfer from the two-phase interface to the subcooled solid

$$C(\tilde{t}) = \int_0^1 \frac{2B}{\tilde{\lambda}} d\tilde{y}. \tag{24}$$

The definition of these three quantities is patterned after equation (14), which integrated from $\tilde{y} = 0$ to 1 reads

$$M = He - C. \tag{25}$$

This relationship between M, He and C is evident also in Fig. 2 (note the logarithmic scale). In the case illustrated in the figure ($A = 1$, $B = 1$, $Ste = 0.1$), the heating and cooling rates are practically equal until $\tilde{t}$ becomes of the order of 1. As a consequence, the melting rate M is negligible with respect to either He or C. The time $\tilde{t} \sim O(1)$ marks the establishment of the convective steady state of the liquid-side boundary layer flow, as was noted immediately under equation (9). At times $\tilde{t} > O(1)$, the roles of M and C are reversed: the effect of conduction into the subcooled solid becomes negligible, as the heating rate He is gradually balanced by the melting rate M. The He and M curves approach the same horizontal asymptote in the 'quasi-steady' regime, in which the finite solid subcooling has become a thing of the past.

5. THE EFFECT OF SOLID SUBCOOLING

There are three parameters—A, B and Ste—that can independently alter the quantitative aspect of the

Table 1. The effect of the time step ($\Delta\tilde{t}$) and the number of steps in the vertical direction (N) on the numerical solution for the liquid-side boundary-layer thickness ($\tilde{\delta}$) ($A = 1$, $B = 1$, $Ste = 0.1$)

	$\tilde{t} = 1$			$\tilde{t} = 5$				
$\tilde{y}$	0.05	0.50	0.95	0.05	0.50	0.95	N	$\Delta\tilde{t}$
$\tilde{\delta}$	1.6730	3.2141	3.4485	1.7043	3.2973	3.9390	21	0.1
	1.7134	3.2511	3.4595	1.734	3.3467	3.9222	31	0.05
	1.7282	3.2794	3.4641	1.7497	3.3294	3.9141	41	0.01

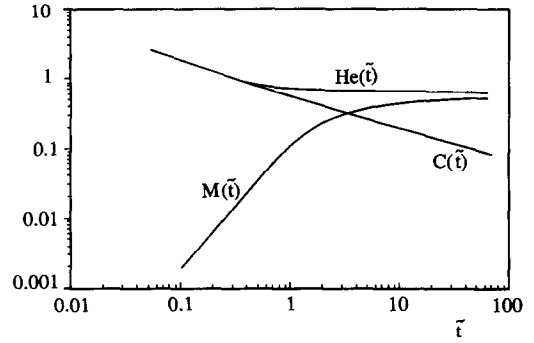

FIG. 2. The competition between the height-averaged heating rate *He*, cooling rate *C*, and melting rate *M*, during the life of the time-dependent phenomenon ($A = 1$, $B = 1$, $Ste = 0.1$).

melting, heating and cooling rate histories. Figure 3 shows how the local melting velocity $\tilde{u}_0(\tilde{y}, \tilde{t})$ responds to an increase in the degree of solid subcooling. In every constant B frame, the instantaneous melting velocity decreases in the downward direction ($\tilde{y}$). The fact that it tends to infinity at the very top of the interface is the fingerprint of the boundary-layer assumption on which the analysis of Section 3 was based. As the time increases, the melting velocity $\tilde{u}_0$ increases also, regardless of the local position $\tilde{y}$ along the two-phase interface. This last trend was indicated earlier by the shape of the melting rate curve M in Fig. 2.

The effect of increasing B can be seen by comparing the three frames of Fig. 3. Generally speaking, higher B values mean lower melting velocities, especially in the early phase of the process. Important to note is the $\tilde{u}_0 = 0$ value plotted on the abscissa: the last frame of Fig. 3 shows that when the subcooling parameter B is large enough, the early phase of the phenomenon is one of solidification ($\tilde{u}_0 < 0$), not melting. At sufficiently large values of $\tilde{t}$, i.e. when the conduction into the subcooled solid has already run its course, melting occurs over the entire height of the interface.

The development of conjugate boundary layers on both sides of the solid–liquid interface is shown in Fig. 4. In each constant B frame, the solid-side boundary layer grows indefinitely as the time increases. This behavior is unlike that on the liquid side, where a steady-state thickness is reached when $\tilde{t}$ exceeds $O(1)$. As B increases from 1 in the upper frame to 10 in the lower frame of Fig. 4, we see that the solid-side boundary layer becomes thicker (compare, for instance, the $\tilde{t} = 60$ curves shown in both frames). On the liquid side, the increase in B leads to a slightly thinner boundary layer, or in view of the *He* integral (23), a slightly higher heating rate.

The effect of solid subcooling on the heating rate is examined in greater detail in Fig. 5. This figure shows that, indeed, the effect of higher B values is to 'slightly' increase the asymptotic *He* value reached in the quasi-steady (or convection-dominated) melting regime. The effect of B is considerably more pronounced when $\tilde{t} < O(1)$, that is, when both sides of the interface are ruled by conduction.

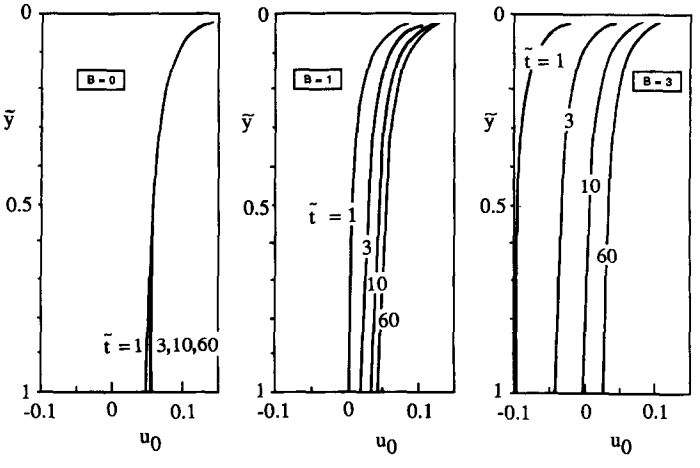

FIG. 3. The effect of the solid subcooling parameter B on the local melting velocity ($A = 1$, $Ste = 0.1$).

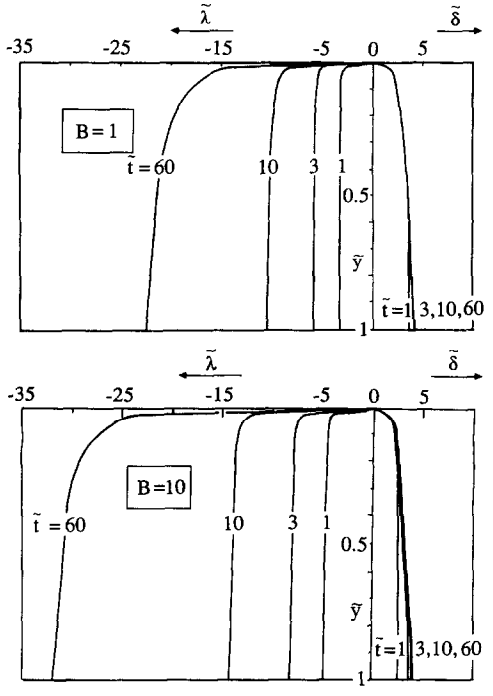

FIG. 4. The effect of the solid subcooling parameter B on the development of the conjugate boundary layers ($A = 1$, $Ste = 0.1$).

The occurrence of solidification when the degree of subcooling is high is documented further in Fig. 6. The top portion of this figure shows how the average melting rate decreases as B increases, and how the effect of B diminishes as the time increases. The $M(\tilde{t})$ curve drawn for $B = 10$ shows that solidification prevails over almost the entire time interval covered by the abscissa.

The lower portion of Fig. 6 shows a more practical counterpart of the average melting rate

$$S = \int_0^{\tilde{t}} M(\tilde{t}_1)\,\mathrm{d}\tilde{t}_1 \tag{26}$$

namely, the total volume swept by the two-phase interface from the start of the process ($\tilde{t} = 0$) until time $\tilde{t}$. A positive S value means that a finite volume

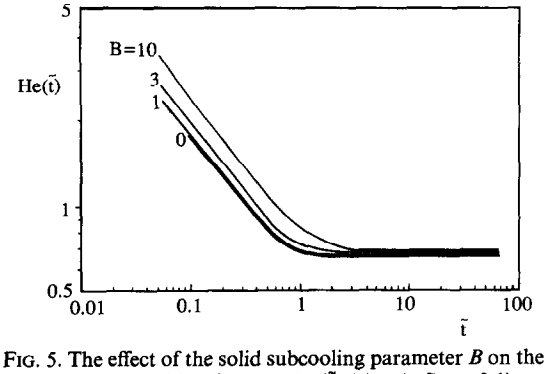

FIG. 5. The effect of the solid subcooling parameter B on the height-averaged heating rate $He(\tilde{t})$ ($A = 1$, $Ste = 0.1$).

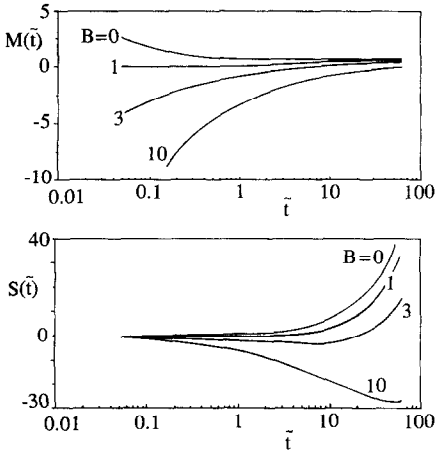

FIG. 6. The effect of solid subcooling on the instantaneous average melting rate (top drawing), and on the total volume swept by the interface (bottom drawing) ($A = 1$, $Ste = 0.1$).

of solid has been converted into liquid. This is the case when the degree of subcooling is small. When B is of the order of 3 or greater, the phase change is of net solidification during the early phase of the process. The effect of early solidification ($S < 0$) is felt over a time interval that is longer than the interval when only the instantaneous melting rate M is negative. In other words, in terms of volume of material that has undergone a phase change, the effect of early solidification is forever a part of the history of the process. Even though melting always takes over after a sufficiently long time, the increase of S with the increasing $\tilde{t}$ is delayed in proportion with B, or with the duration of the early period of solidification.

In the preceding discussion, we referred to higher B values as an indication of a larger degree of subcooling in the solid. This is correct when the thermal conductivity ratio k_s/k_f is fixed, as in the single material used in the experiment described in Section 8. The parameter B can increase also when the degree of subcooling (or the ratio $\Delta T_s/\Delta T_f$) is fixed. In this case, higher values of B are associated with a sequence of materials that have increasingly larger thermal conductivity ratios. The conclusion drawn based on Figs. 3–6 holds in this case as well.

6. THE EFFECT OF THE THERMAL DIFFUSIVITY RATIO

We turn now to the thermal diffusivity ratio, $A = \alpha_s/\alpha_f$, and the role that it plays in the time-dependent melting/solidification process. The most interesting effect is displayed in the top of Fig. 7, which shows the history of the instantaneous melting rate M in a case with finite subcooling in the solid ($B = 1$). As the A ratio decreases, the $M(\tilde{t})$ curve is pushed downward into the 'solidification' domain. The process crosses eventually into the melting domain, $M > 0$, however, the time of this change is delayed as A decreases.

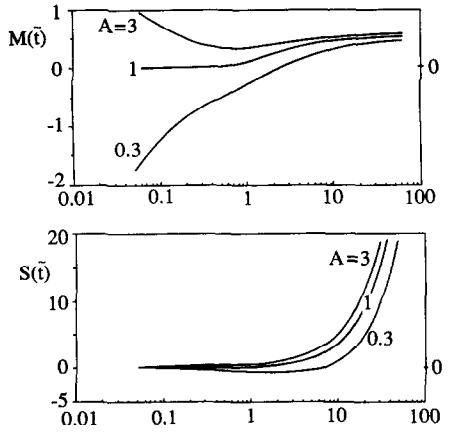

FIG. 7. The effect of the thermal diffusivity ratio on the instantaneous average melting rate (top drawing), and on the total volume swept by the interface (bottom drawing) ($B = 1$, $Ste = 0.1$).

The corresponding curves showing the history of the volume swept by the interface are plotted in the lower part of Fig. 7. The A effect is the same, except that the cross-over into the 'net melting' domain ($S > 0$) occurs long after the instantaneous melting rate has changed sign (see, e.g. the $A = 0.3$ curves on both parts of Fig. 7).

Figure 8 shows that the diffusivity ratio has practically no effect on the average heating rate He during the convection-dominated regime, $\tilde{t} > O(1)$. This feature is another sign that the loss of heat by conduction into the solid has already diminished. More surprising is that even during the early phase, $\tilde{t} < O(1)$, when the solid-body conduction phenomenon is important, the diffusivity ratio A has only a minor impact on $He(\tilde{t})$.

7. THE EFFECT OF LIQUID SUPERHEATING

The effect of the liquid-side Stefan number is relatively better understood, thanks to several studies of natural convection melting in enclosed phase-change materials (for a tabular summary of these studies, see ref. [4]). For this reason, in this paper we show only

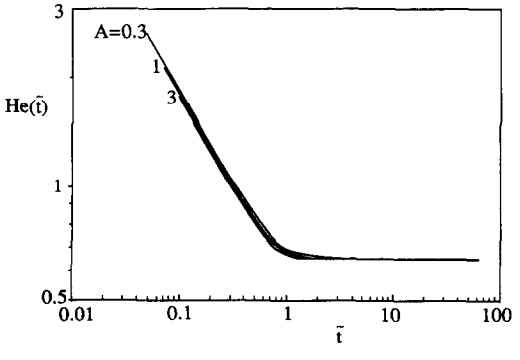

FIG. 8. The effect of the thermal diffusivity ratio on the instantaneous average heating rate ($B = 1$, $Ste = 0.1$).

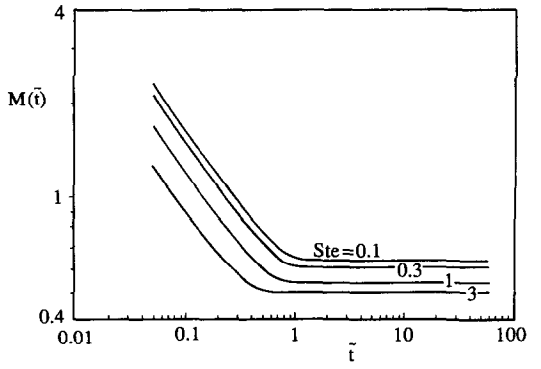

FIG. 9. The effect of liquid superheating (Ste) on the instantaneous average melting rate ($A = 1$, $B = 0$).

the melting rate history (Fig. 9), and how the $M(\tilde{t})$ curve shifts downward and to the left as Ste increases. The Ste effect is sizeable throughout the time interval covered in Fig. 9, however, it is most pronounced during the early period, when the growth of the liquid-side thermal boundary layer is ruled by transient conduction.

In conclusion, the melting rate decreases as the Stefan number increases. This trend agrees with the trend observed in the melting of encapsulated materials [4]. Its explanation lies in the fact that when Ste increases, a greater fraction of the heating effect that is available at the interface must be set aside for the 'sensible' heating of the newly created liquid. The boundary layer becomes thicker as Ste increases.

8. EXPERIMENT

The principal objective of this study was to document the manner in which the solid subcooling parameter B influences the main quantities that compete at the interface, the heating rate He, the melting rate M, and the cooling rate C. In this section we report a qualitative test of the predicted B effect. This test was conducted in an experiment where an enclosed amount of n-octadecane was heated at a constant rate.

The description of the experimental apparatus is given in great detail in ref. [23], therefore, it will not be repeated here. Figure 10 shows that the vertical cross-section of the enclosure is a rectangle with height $H = 0.74$ m and width 0.146 m. The depth of the enclosure is 0.56 m: this third dimension is sufficiently large to minimize the three-dimensional features of the liquid flow and two-phase interface.

The two large side walls are made out of 1.8 cm thick aluminum plate. One of these plates can be heated at a constant rate (in time) by means of eight equidistant resistive strip heaters. The other large wall can be cooled by a stream of alcohol supplied by a constant-temperature bath system. The enclosure is surrounded by a 15 cm thick layer of fiberglass insulation, and, as a consequence, the overall heat loss from the enclosure is less than 1.5% of the total heating rate supplied by the eight electric heaters. The

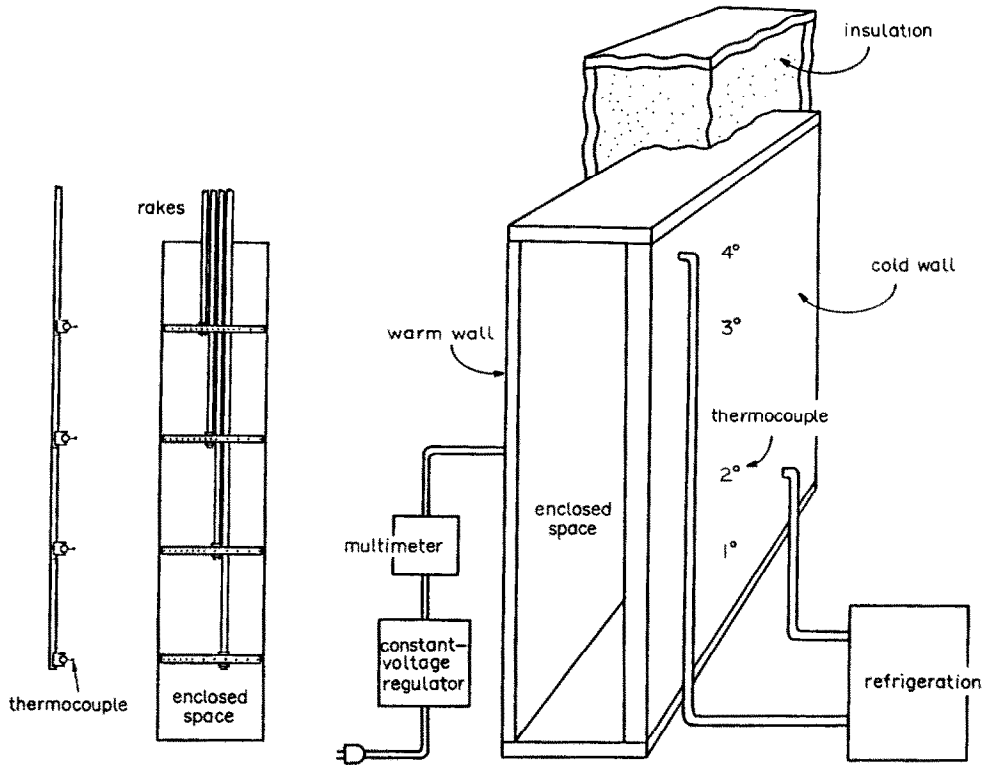

FIG. 10. Scale drawing of the vertical cross-section of the experimental apparatus.

remaining four walls of the enclosure (top, bottom, front, back) are made of out 2.5 cm thick acrylic plexiglas sheet.

The time-dependent temperature distributions along the two aluminum plates were measured by means of thermocouples positioned at four altitudes in the vertical midplane of the apparatus. The history of the distribution of temperature in the solid and liquid regions was monitored with 55 chromel–alumel (type K) thermocouples held by four horizontal rakes. The accuracy of each temperature reading was within $\pm 0.1°C$.

The purpose of the original experiment for which the apparatus was built [23] was to study the constant-rate melting of an enclosed solid with zero subcooling. In the present series of experiments, the objective was to study the effect of the subcooling parameter B. Each run started from a state of finite solid subcooling, so that the entire B range covered by these runs is approximately 0.3–6.3 (Fig. 11 inset). In the beginning, the enclosure was filled with solid n-octadecane.

Owing to the persistence of slight deviations from the desired isothermal state at the start of each melting run, the uncertainty associated with the B values reported in Fig. 11 is of the order of $\pm 4\%$. The heating rate was the same in all the runs, in other words, the heat-flux Rayleigh number Ra_* did not change from one run to the next

$$Ra_* = \frac{g\beta H^4 q''}{\alpha \nu k_f} = (2.34)10^{13}. \qquad (27)$$

The relationship between Ra_* and the more common Rayleigh number based on the temperature difference (e.g. equation (9)) will be discussed shortly.

Figure 11 shows the evolution of the average temperature of the heated wall, T_{avg}. This temperature was calculated by first curve-fitting the wall temperature measurements provided by the four thermocouples, and then averaging over the entire height H the resulting temperature distribution. The figure illustrates three important features:

(a) the early period of the process is one in which the heated wall temperature increases,

(b) the late period is characterized by a wall temperature that is nearly constant in time, and

(c) the early-period temperatures are progressively lower as the degree of solid subcooling (B) increases from one run to the next.

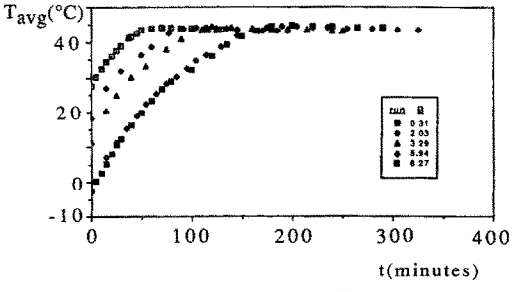

FIG. 11. The effect of the solid subcooling parameter B on the history of the heated-wall temperature.

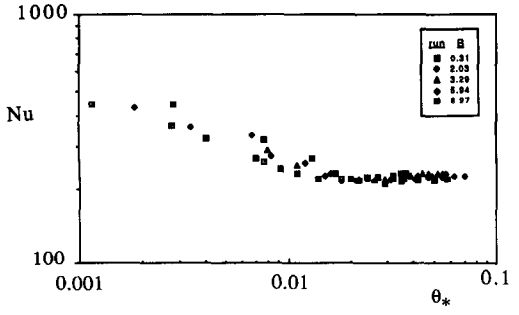

FIG. 12. The effect of solid subcooling on the overall Nusselt number during constant-rate heating experiments.

The same features are visible also in the dimensionless counterpart of Fig. 11, namely, the overall Nusselt number shown in Fig. 12

$$Nu = \frac{q''H}{k_f(T_{avg} - T_m)}. \tag{28}$$

The uncertainty associated with the reported values of Nu as well as with the value of Ra_* from equation (27) is of the order of $\pm 3\%$. The time plotted on the abscissa, θ_*, is a proper dimensionless time for constant-rate heating experiments [23]

$$\theta_* = \frac{q''t}{\rho h_{sf} H}. \tag{29}$$

The subcooling parameter B appears to be responsible for the apparent scatter exhibited by the data taken during the early period, that is, before the liquid circulation is characterized by quasi-steady and distinct boundary layers. At a fixed time θ_* in the early period, the Nusselt number increases by approximately 20% as B increases from 0.3 to 6.3. This increase is very similar to the trend seen already in the early period of the $He(\hat{t})$ curves plotted in Fig. 5. In both Figs. 12 and 5, the subcooling parameter B appears to have no effect in the late period of the process, that is, in the convection or quasi-steady regime.

9. DISCUSSION

The agreement between the B trends exhibited in Figs. 12 and 5 can be used for the purpose of correlating the experimental data of Fig. 12. To begin with, it is important to note the relationship between the overall Nusselt number Nu revealed by experiments, and the overall heating rate He plotted in Fig. 5. The latter refers to the heat transfer received by the interface between the solid phase and an isothermal pool of liquid, across the temperature difference ΔT_f. In the experiment, the role of ΔT_f is played by the difference between the average temperature of the liquid zone and the melting front temperature. This difference, in turn, is roughly equal to half of the difference between the average wall temperature (T_{avg}) and the melting front temperature (T_m). Therefore, in order to compare quantitatively the heat transfer results plotted in Figs. 5 and 12, we set

$$\Delta T_f \cong \tfrac{1}{2}(T_{avg} - T_m). \tag{30}$$

Next, we note that the analysis that led to Fig. 5 employed the Rayleigh number (Ra) based on ΔT_f. Taking the quasi-steady regime measurements of Fig. 11 as a representative order of magnitude of T_{avg}, we rely on equations (30) and (9) in order to calculate the experimental value of the ΔT_f-based Rayleigh number

$$Ra \cong (0.51)10^{10}. \tag{31}$$

Let q' [W m^{-1}] be the total (height-integrated) heat transfer rate from the liquid into the two-phase interface. The He definition (23) can then be rewritten as

$$\frac{q'}{k_f \Delta T_f} = Ra^{1/4}\, He. \tag{32}$$

On the experimental side of the argument, q' is the same as the product $q''H$ of equation (28); therefore, by combining equations (28) and (30) we can write also

$$\frac{q'}{k_f \Delta T_f} \cong 2Nu. \tag{33}$$

Equations (32) and (33) show that a direct comparison can be made between the $Ra^{1/4}\,He$ values of Fig. 5 and the experimental $2Nu$ value of Fig. 12, or between He and the group $2Nu\,Ra^{-1/4}$. Taking the quasi-steady regime measurements $Nu \cong 230$ as representative of the order of magnitude of the Nusselt number, the experimental quantity equivalent to He becomes

$$2Nu\,Ra^{-1/4} \cong 0.97. \tag{34}$$

This value is definitely of the same order of magnitude as the $He \cong 0.7$ plateau reached by He in the quasi-steady regime of Fig. 5. In conclusion, the theoretical results and the experimental measurements agree not only with respect to the trends they reveal, but also in an order of magnitude sense.

The theoretical $He(\hat{t})$ curves of Fig. 5 are such that they fall on top of the same curve if they are shifted appropriately in the plane of the figure. The larger part of this shift amounts to a translation of the curve in the horizontal direction. In view of the logarithmic scale, the horizontal translation can be achieved by dividing the abscissa coordinate by the group $(1+KB)$, in which K is an empirical constant. This idea was used in order to correlate the B effect that is so evident in the small θ_* part of Fig. 12. The result of this effort is presented in Fig. 13, in which the new abscissa parameter $\theta_*/(1+1.28B)$ accounts for the effect of solid subcooling.

Finally, the conciseness of the analytical work described in Sections 2–4 is due mainly to the simplifying assumptions on which it is based. Key among these is the assumption that the liquid–solid interface

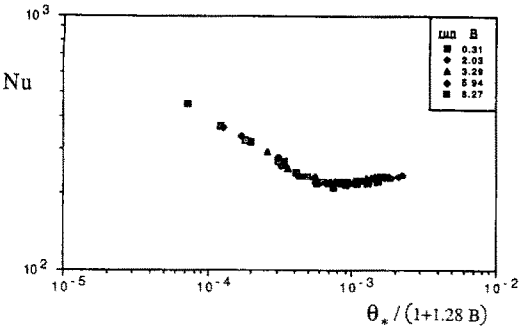

FIG. 13. The correlation of the effect of solid subcooling on the experimental data of Fig. 12.

remains plane and nearly vertical. This assumption breaks down as the time increases, because the uneven melting rate u_0 creates an interface the shape of which resembles the shape of the $\tilde{u}_0(\tilde{y})$ curves displayed in Fig. 3. This shape, however, should not be confused with the actual displacement (deflection, amplitude) of the interface: the displacement is described by the function $s(y, t)$, which is discussed next.

The time interval in which the boundary-layer analysis is valid can be determined by reasoning that, in it, the order of magnitude of the slope of the deflected interface is small

$$\frac{\partial s}{\partial y} < 1. \tag{35}$$

In this argument, $s(y, t)$ is the function describing the instantaneous shape of the interface, i.e. the travel of the interface toward the left in Fig. 1. As time increases, the melting process reaches the quasi-steady (convection) regime, in which s is proportional to both $u_0(y, t)$ and t

$$s = u_0 t. \tag{36}$$

Therefore, in the dimensionless notation defined in equations (7)–(9), the small-slope criterion (35) becomes a 'time' criterion

$$\tilde{t} < \frac{Ra^{1/4}}{(\partial \tilde{u}_0/\partial \tilde{y})}. \tag{37}$$

This time criterion shows, first, that the theoretical solution always breaks down near the tip of the boundary layers ($\tilde{y} = 0$), where the denominator $\partial \tilde{u}_0/\partial \tilde{y}$ of equation (37) is very large. This limitation is consistent with the boundary-layer theory invoked in writing governing equations (2) and (3): that theory breaks down near $\tilde{y} = 0$ also.

Figure 3 shows that the slope $\partial \tilde{u}_0/\partial \tilde{y}$ is finite and much smaller than 1 over most of the height of the two-phase interface. This means that the time interval $\tilde{t}$ in which the conjugate boundary-layer analysis is valid, is a finite number that increases as $Ra^{1/4}$ increases. This aspect is examined in closer detail in a purely analytical study of the circulation in the liquid cavity and the interface melting in the absence of solid subcooling [24, 25].

Acknowledgement—This work was supported by the Electric Power Research Institute through contract No. RP 8006-4, under the management of Dr Jong H. Kim.

REFERENCES

1. M. Epstein and D. H. Cho, Melting heat transfer in steady laminar flow over a flat plate, *J. Heat Transfer* **98,** 531–533 (1976).
2. M. Epstein and D. H. Cho, Laminar film condensation on a vertical melting surface, *J. Heat Transfer* **98,** 108–113 (1976).
3. R. L. Reid, Integral methods for the melting of permafrost by groundwater flow, 15th National Heat Transfer Conf., Paper AIChE 32E10-G7, San Francisco, California, August (1975).
4. B. W. Webb and R. Viskanta, On the characteristic length scale for correlating melting heat transfer data, *Int. Commun. Heat Mass Transfer* **12,** 637–646 (1985).
5. P. Jany and A. Bejan, Scaling theory of melting with natural convection in an enclosure, *Int. J. Heat Mass Transfer* **31,** 1221–1235 (1988).
6. R. Viskanta, Natural convection melting and solidification. In *Natural Convection: Fundamentals and Applications* (Edited by S. Kakac, W. Aung and R. Viskanta). Hemisphere, Washington, DC (1985).
7. N. W. Hale and R. Viskanta, Photographic observation of the solid–liquid interface motion during melting of a solid heated from an isothermal vertical wall, *Lett. Heat Mass Transfer* **5,** 329–337 (1978).
8. P. D. van Buren and R. Viskanta, Interferometric measurement of heat transfer during melting from a vertical surface, *Int. J. Heat Mass Transfer* **23,** 568–571 (1980).
9. M. Okada, Melting from a vertical plate between insulated top and bottom surfaces, *Proc. ASME/JSME Thermal Engng Joint Conf.*, Vol. 1, pp. 281–288 (1983).
10. M. Okada, Analysis of heat transfer during melting from a vertical wall, *Int. J. Heat Mass Transfer* **27,** 2057–2066 (1984).
11. C. J. Ho and R. Viskanta, Heat transfer during melting from an isothermal vertical wall, *J. Heat Transfer* **106,** 12–19 (1984).
12. M. Bareiss and H. Beer, Experimental investigation of melting heat transfer with regard to different geometric arrangements, *Int. Commun. Heat Mass Transfer* **11,** 323–333 (1984).
13. C. Bénard, D. Gobin and F. Martinez, Melting in rectangular enclosures: experiments and numerical simulation, *J. Heat Transfer* **107,** 794–803 (1985).
14. C. Gau and R. Viskanta, Melting and solidification of a pure metal on a vertical wall, *J. Heat Transfer* **108,** 174–180 (1986).
15. A. Kassinos and J. Prusa, Effects of density change and subcooling on the melting of a solid in a rectangular enclosure. In *Heat Transfer 1986*, Vol. 4, pp. 1787–1792. Hemisphere, Washington, DC (1986).
16. A. Bejan, *Convection Heat Transfer*. Wiley, New York (1984).
17. E. M. Sparrow, W. J. Minkowycz and M. Saddy, Forced convection condensation in the presence of noncondensables and interfacial resistance, *Int. J. Heat Mass Transfer* **10,** 1829–1845 (1967).
18. H. B. Squire, Integral solution published in *Modern Developments in Fluid Dynamics* (Edited by S. Goldstein), Vol. 2, pp. 641–643. Dover, New York (1965).
19. P. A. Blythe and P. G. Simpkins, Thermal convection in a rectangular cavity, *PhysicoChem. Hydrodyn.* **2,** 511–524 (1977).
20. R. Eichhorn, The effect of mass transfer on free convection, *J. Heat Transfer* **82,** 260–263 (1960).

21. L. S. Yao and W. Cherney, Transient phase-change around a horizontal cylinder, *Int. J. Heat Mass Transfer* **24**, 1971–1981 (1981).
22. J. Prusa and L. S. Yao, Effects of density change and subcooling on the melting of a solid around a horizontal heated cylinder, *J. Fluid Mech.* **155**, 193–212 (1985).
23. Z. Zhang and A. Bejan, Melting in an enclosure heated at constant rate, *Int. J. Heat Mass Transfer* **32**, 1063–1076 (1989).
24. A. Bejan, Theory of melting with natural convection in an enclosed porous medium, *J. Heat Transfer* **111**, 407–415 (1989).
25. A. Bejan, Analysis of melting by natural convection in an enclosure, *Int. J. Heat Fluid Flow* (1989), in press.

LE PROBLEME DE LA FUSION VARIABLE EN CONVECTION NATURELLE AVEC CONDUCTION DANS LE SOLIDE

Résumé—On étudie thermiquement et expérimentalement l'effet du sous-refroidissement, du côté solide, sur le phénomène du fusion par convection naturelle à l'interface vertical entre un solide et un bain liquide de même nature. La première partie de l'étude consiste en l'analyse du mécanisme de fusion variable, dans lequel l'effet du sous-refroidissement du solide conduit à une couche limite de conduction variable dans le solid. La solution théorique traite aussi de l'effet de la surchauffe du liquide (nombre de Stefan) et du rapport de diffusivité thermique. La seconde partie de l'étude concerne des expériences faites avec une cavité rectangulaire chauffée à flux constant sur le côté. Le paramètre de sous-refroidissement du solide B couvre le domaine 0,3–6,3, tandis que le nombre de Rayleigh reste constant. Les expériences montrent que dans le régime dominé par la conduction, le nombre de Nusselt augmente quand B croît. Dans le régime dominé par la convection, l'effet de B est insignifiant. On montre que ces observations expérimentales s'accordent avec les tendances dégagées théoriquement dans la première partie de l'étude.

DER ZEITABHÄNGIGE SCHMELZVORGANG BEI NATÜRLICHER KONVEKTION MIT WÄRMELEITUNG IM FESTSTOFF

Zusammenfassung—Diese Arbeit beschreibt eine theoretische und experimentelle Untersuchung des Einflusses der feststoffseitigen Unterkühlung auf das Schmelzen bei natürlicher Konvektion an der vertikalen Grenzfläche zwischen fester und flüssiger Phase. Der erste Teil der Arbeit besteht aus einer Analyse der Grenzschicht beiderseits der Phasengrenze des transienten Schmelzprozesses, wenn die Unterkühlung der festen Phase zu einer zeitabhängigen Wärmeleitungsgrenzschicht im Feststoff führt. Die Ergebnisse der theoretischen Untersuchung zeigen sowohl den Einfluß der Unterkühlung der festen Phase auf die Schmelzgeschwindigkeit als auch diejenigen Einflüsse der Überhitzung der flüssigen Phase (Stefan-Zahl) und des Verhältnisses der Temperaturleitfähigkeiten. Der zweite Teil der Arbeit besteht aus Schmelzexperimenten, welche in einem rechteckigen, geschlossenen, seitlich gleichförmig beheizten Hohlraum durchgeführt wurden. Der Parameter der Unterkühlung der festen Phase (B) bewegt sich bei konstanter Rayleigh-Zahl im Bereich von 0,3–6,3. Die Experimente zeigten, daß in dem von Wärmeleitung dominierten Bereich die Nusselt-Zahl mit steigendem B zunimmt. In dem von Konvektion dominierten Bereich ist der Einfluß des Unterkühlungsparameters B nicht von Bedeutung. Es wird gezeigt, daß diese experimentellen Beobachtungen qualitativ mit den Ergebnissen aus dem theoretischen ersten Teil der Studie übereinstimmen.

ИССЛЕДОВАНИЕ НЕСТАЦИОНАРНОГО ПРОЦЕССА ПЛАВЛЕНИЯ ПРИ ЕСТЕСТВЕННОЙ КОНВЕКЦИИ С УЧЕТОМ ТЕПЛОПРОВОДНОСТИ В ТВЕРДОМ ТЕЛЕ

Аннотация—Теоретически и экспериментально исследуется влияние недогрева твердого тела на плавление при естественной конвекции на вертикальной границе между твердым телом и его жидкой фазой. Первая часть посвящена сопряженному анализу теплообмена при плавлении, когда эффект недогрева твердого тела приводит к образованию в нем нестационарного теплового пограничного слоя. В теоретическом решении учитываются не только влияние недогрева твердого тела на интенсивность плавления, но и эффекты перегрева жидкости (число Стефана) и отношение температуропроводностей. Во второй части исследования содержится описание экспериментов, проводимых в прямоугольной полости с постоянным подводом тепла к боковой поверхности. Параметр недогрева твердого тела B изменяется в диапазоне 0,3–6,3, в то время как число Рэлея остается постоянным. Эксперименты показывают, что в определяемом теплопроводностью режиме плавления число Нуссельта увеличивается с ростом параметра недогрева B. При режиме, определяемом конвекцией, эффект этого параметра незначителен. Показано, что экспериментальные данные подтверждают закономерности, рассчитанные теоретически в первой части работы.